Cell Reports
Report

Target-Derived Matricryptins Organize Cerebellar Synapse Formation through α3β1 Integrins

Jianmin Su,[1] Renee S. Stenbjorn,[1] Karen Gorse,[1] Kaiwen Su,[1] Kurt F. Hauser,[2] Sylvie Ricard-Blum,[3] Taina Pihlajaniemi,[4,5,6] and Michael A. Fox[1,*]
[1]Department of Anatomy and Neurobiology
[2]Department of Pharmacology and Toxicology
Virginia Commonwealth University, Richmond, VA 23298, USA
[3]Institut de Biologie et de Chimie des Protéines, UMR 5086 CNRS, University Lyon 1, Cedex 07, Lyon 69367, France
[4]Oulu Center for Cell-Matrix Research
[5]Biocenter Oulu
[6]Department of Medical Biochemistry and Molecular Biology
University of Oulu, Oulu 90014, Finland
*Correspondence: mafox@vcu.edu
http://dx.doi.org/10.1016/j.celrep.2012.07.001

SUMMARY

Trans-synaptic organizing cues must be passed between synaptic partners for synapses to properly form. Much of our understanding of this process stems from studies at the neuromuscular junction, where target-derived growth factors, extracellular matrix (ECM) molecules, and matricryptins (proteolytically released fragments of ECM molecules) are all essential for the formation and maintenance of motor nerve terminals. While growth factors and ECM molecules also contribute to the formation of brain synapses, it remains unclear whether synaptic roles exist for matricryptins in the mammalian brain. We report that collagen XVIII and its matricryptin endostatin are generated by cerebellar Purkinje cells and are necessary for the organization of climbing fiber terminals in these neurons. Moreover, endostatin is sufficient to induce climbing fiber terminal formation in vitro by binding and signaling through α3β1 integrins. Taken together, these studies reveal roles for both matricryptins and integrins in the organization of brain synapses.

INTRODUCTION

Synapses, which allow the transfer of information between cells in the nervous system, begin to form when growing axons contact appropriate target cells. After initial contact, molecular signals are passed between synaptic partners to transform the axon and postsynaptic target into a synapse. First insight into the molecular signals that mediate this process (termed synaptic differentiation) came from studies at the neuromuscular junction (NMJ), where *trans*-synaptic cues, in the form of growth factors, morphogens, and extracellular matrix (ECM) molecules, induce pre- and postsynaptic differentiation (Fox and Umemori, 2006). Recent studies have further demonstrated that proteolytically released fragments of ECM molecules also contribute to NMJ formation (Fox et al., 2007). Specifically, controlled proteolysis of several collagen molecules generates soluble peptides, termed matricryptins, that exhibit unique bioactivities compared to the full-length molecule from which they are derived (Ricard-Blum and Ballut, 2011). At the NMJ, collagen IV-derived matricryptins direct the assembly and maintenance of motor nerve terminals (Fox et al., 2007).

Despite anatomical differences, the formation of central synapses is remarkably similar to that of the NMJ in that *trans*-synaptic cues direct synaptic differentiation (Fox and Umemori, 2006). In fact, many of the same families of molecules that direct NMJ formation contribute to synapse formation in the brain. Examples include Wnts, FGFs, agrin, and laminins (Terauchi et al., 2010; Ksiazek et al., 2007; Egles et al., 2007). It remains unclear, however, whether roles for matricryptins exist at central synapses. Here, we screened for matricryptin-releasing collagens in brain and discovered that cerebellar Purkinje cells express collagen XVIII. Using in vivo and in vitro approaches, we show that collagen XVIII is necessary for the organization of climbing fiber (CF) terminals, and endostatin—the matricryptin released from this collagen—is sufficient to induce their formation.

RESULTS AND DISCUSSION

Matricryptin Expression in Cerebellum

To assess whether matricryptins are present in the mammalian brain, we screened for collagen gene expression in mouse brain. One collagen gene, *col18a1* (which encodes collagen XVIII), was exclusively enriched in cerebellum (Figure 1A). Outside of the nervous system, three *col18a1* isoforms are expressed in tissue-specific manners (Muragaki et al., 1995); however, we found that all were expressed in cerebellum (Figures S1A and S1B). Using primers and riboprobes that detect all *col18a1* isoforms, we found that expression coincides with synaptogenesis (Figure 1B) and is restricted to a single class of neurons—Purkinje cells (Figures 1C, 1D, and S1C).

Collagen XVIII is a heparan sulfate proteoglycan and harbors a C-terminal matricryptin termed endostatin. Outside of the

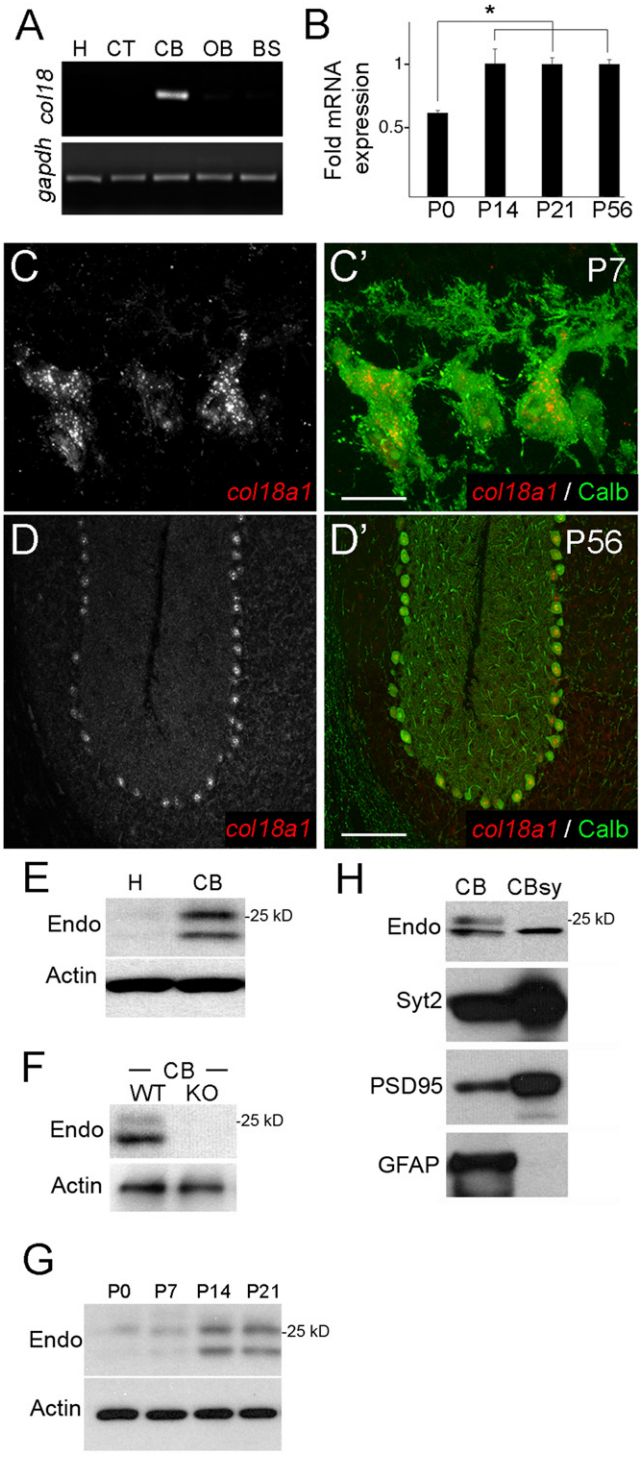

Figure 1. Expression of Collagen XVIII/Endostatin in Mouse Cerebellum

(A) RT-PCR for *col18a1* and *gapdh* mRNAs from RNA isolated from P56 mouse hippocampus (H), cerebral cortex (CT), cerebellum (CB), olfactory bulb (OB), and brain stem (BS).

(B) qPCR show *col18a1* mRNA expression is developmentally regulated. Expression levels normalized to *gapdh*. Data shown are means ± SD; n > 3 per age. *Differs from P0 at $p < 0.003$ by one-way analysis of variance (ANOVA).

(C and D) In situ hybridization show *col18a1* expression is restricted to calb-expressing Purkinje cells. Scale bar in (C), 15 μm; in (D), 150 μm.

(E) WBs demonstrate endostatin (endo)-containing fragments of collagen XVIII in P56 cerebellar protein extracts.

(F) WBs of wild-type (WT) and *col18a1*$^{-/-}$ mutant (KO) CB extracts demonstrate antibody specificity.

(G) WBs show levels of endostatin-containing peptides are developmentally regulated. Actin is a loading control for (E–G).

(H) WBs demonstrate a 20 kDa endostatin-containing fragment is present in cerebellar synaptosome fractions (CBsy). CBsy lack nonsynaptic proteins, such as GFAP, and are enriched for synaptic proteins (e.g., PSD95, Syt2).

nervous system, endostatin shares functional similarities with those collagen IV-derived matricryptins that organize NMJ formation (Ricard-Blum and Ballut, 2011). In addition to these similarities with synaptogenic matricryptins, endostatin was a good candidate to direct synaptogenesis in the mammalian brain since it regulates neuromuscular circuit formation in worms, flies, and fish (Ackley et al., 2003, Meyer and Moussian, 2009; Schneider and Granato, 2006). We therefore asked whether endostatin contributes to cerebellar circuit formation.

To answer this question, we began by assessing whether endostatin protein was present in cerebellum. Western blots (WBs) with an antibody that specifically react with the endostatin domain of collagen XVIII revealed two endostatin-containing peptides (~20 and 25 kDa) were present in cerebellum (Figure 1E). These fragments were absent from other brain regions and from cerebellum of mice lacking collagen XVIII (*col18a1*$^{-/-}$) (Figures 1E and 1F). Similar to mRNA levels, increases in endostatin levels coincided with synaptogenesis (Figure 1G). Unfortunately anti-endostatin antibodies worked poorly for localizing this matricryptin in brain tissue. To circumvent this problem, we probed for endostatin in cerebellar synaptosomes—biochemical fractions enriched for synaptic elements. A single 20 kDa endostatin-containing fragment appeared present in cerebellar synapses (Figures 1H and S1D), suggesting that cleavage of endostatin from collagen XVIII may be different in synaptic and extrasynaptic compartments of the cerebellum. Together, these results demonstrate not only that Purkinje cells generate collagen XVIII/endostatin during synapse formation but also that endostatin is present at cerebellar synapses.

Collagen XVIII/Endostatin Is Necessary for CF Terminal Formation

Based on the role of matricryptins at the NMJ, we hypothesized that endostatin may be necessary to organize nerve terminal assembly on to Purkinje cell dendrites. Nerve terminals from four types of neurons synapse on to Purkinje cells: Parallel fibers (PFs), which originate from granule cells, form excitatory terminals on to dendritic spines of Purkinje cell dendrites; basket cells (BCs) form inhibitory terminals on to the Purkinje cell soma and axon initial segment; stellate cells (SCs) form inhibitory terminals on to Purkinje cell dendrites; and CFs originate from inferior olivary neurons and form excitatory terminals on the proximal shaft of Purkinje cell dendrites (Figure 2A) (Sotelo, 2008). Since there is no method to eliminate matricryptins without affecting full-length collagen (because of the necessity of C-terminal matricryptins for collagen trimerization within the endoplasmic reticulum), we assessed synapses in *col18a1*$^{-/-}$ mutants, which lack both

collagen XVIII and endostatin. These mutants are viable and have morphologically normal cerebella (Figure S2).

To visualize different subsets of nerve terminals on Purkinje cell dendrites, we immunostained cerebellar tissue with antibodies directed against distinct isoforms of nerve-terminal-associated proteins (Figure 2B). PF terminals were labeled with antibodies against vesicular glutamate transporter 1 (VGluT1) or Bassoon (Fremeau et al., 2001; Richter et al., 1999). To label inhibitory terminals, we used antibodies against synaptotagmin 2 (Syt2), a synaptic vesicle-associated protein expressed by interneurons within the cerebellar molecular layer (and in a population of PF terminals) (Figures 2B, S3, and S4) (Fox and Sanes, 2007). We detected no remarkable difference in the density or distribution of VGluT1, Bassoon, or Syt2 in *col18a1*$^{-/-}$ mutants or littermate controls (Figures 2C–2K). Last, to label CF terminals, we used antibodies against VGluT2 (Fremeau et al., 2001) (Figures 2B and S4). We observed a dramatic and statistically significant decrease in the number of VGluT2-containing varicosities in the molecular layer of mutant cerebella (Figures 2L–2N). Not only were fewer VGluT2-rich varicosities observed, but also VGluT2 appeared diffusely distributed throughout mutant CFs rather than being aggregated into distinct varicosities (Figures 2L and 2M). The abnormal distribution of VGluT2, together with little change in its expression pattern (Figures 2O and 2P), suggested that collagen XVIII/endostatin is critical for the clustering of presynaptic elements into nerve terminals, a hallmark feature of presynaptic differentiation. Based on these defects in synaptic organization, we asked whether *col18a1*$^{-/-}$ mutants exhibit motor dysfunction in a standard accelerating rotarod test (Shiotsuki et al., 2010). *Col18a1*$^{-/-}$ mutants performed significantly worse than controls in this assay (Figure 2Q), a phenotype that suggests (but does not prove) cerebellar defects.

Based upon the organizing role of collagen-derived matricryptins at the NMJ, we hypothesized that reduced numbers of VGluT2-containing CF terminals and motor deficits in *col18a1*$^{-/-}$ mutants arose as a result of endostatin's role in inducing presynaptic differentiation. However, CFs initially arborize around the Purkinje cell somas and then subsequently "climb" the proximal shaft of Purkinje cell dendrites (Mason and Gregory, 1984). Therefore, an alternative possibility was that synaptic defects in *col18a1*$^{-/-}$ mutants arose indirectly due to defects in Purkinje cell dendritogenesis or the ability of CFs to ascend these dendrites. To explore these possibilities, we performed morphological characterizations of Purkinje cell dendrites and CF arbors. Purkinje cell dendrites were labeled by Golgi impregnation, a method in which a small percentage of cerebellar cells were labeled stochastically (Figures S2E and S2F). Areas occupied by individual Purkinje cell dendrites and branch densities of these dendrites appeared indistinguishable in mutant and control cerebella (Figures S2G and S2H).

To address whether CFs properly contacted and ascended Purkinje cell dendrites in *col18a1*$^{-/-}$ mutants, we explored whether CF terminals formed on Purkinje cells in mutants. Colabeling with antibodies against calbindin and VGluT2 revealed that, although fewer VGluT2-containing CF terminals were present in mutant cerebellum, terminals that were present had correctly targeted Purkinje cell dendrites (Figures 2R and 2S). To assess whether CFs ascended Purkinje cell dendrites in mutants, we examined whether CF terminals extended as far into the molecular layer as in controls. VGluT2-containing nerve terminals extended up through ~75% of the molecular layer in controls (Figure 2T). Although fewer VGluT2-containing varicosities were observed in mutants, those varicosities present appeared through an equivalent percentage of the molecular layer (Figure 2T). These two findings suggest that CFs were capable of targeting and "climbing" Purkinje cell dendrites in the absence of collagen XVIII/endostatin. However, to assess their morphology definitively, we anterogradely labeled CFs with lipophilic cyanine dye (DiI) in P20 mutants and controls (Figures 2U and 2V). The average length of CF arbors and the proportion of molecular layer that they crossed were unaltered in *col18a1*$^{-/-}$ mutants (Figures 2W and 2X). Taken together, these studies reveal that reduced numbers of VGluT2-immunoreactive terminals did not result from altered Purkinje cell or CF morphology.

Endostatin Induces CF Terminal Formation In Vitro

To address whether Purkinje cell-derived endostatin was capable of inducing CF nerve terminal formation, we generated dissociated cultures from the inferior olivary nucleus. Since cells in this nucleus do not express *col18a1*, these cultures lack endogenous endostatin (Figure S5). We therefore assessed whether the application of recombinant endostatin onto these neurons affected their CFs in vitro. Application of endostatin had no appreciable affect on the number or morphology of CF-generating inferior olivary neurons (data not shown), which were identified by their expression of calbindin (Calb) (Figure 3A). As we were interested in the axons (and not dendrites) of these neurons, we labeled axons with antibodies against neurofilament (NF), which predominantly labeled CF axons and not other cells in our cultures based on their coexpression of Calb (89.6% ± 2.1% [SD] of NF-expressing neurons' coexpressed Calb; N = 4 experiments; n = 416 neurons) (Figure 3B). Application of endostatin on to these cultures produced a robust increase in the clustering of VGluT2-immunoreactive terminals on NF-positive CFs (Figures 3C–3E and 3H). It is important to note that the presence of endostatin in vitro had no significant affect on mRNA expression levels of *vglut2* (Figure 3I), indicating that endostatin was not merely altering VGluT2 production. Moreover, endostatin-induced varicosities not only contained VGluT2 but also contained other synaptic vesicle-associated proteins such as SV2 and synaptophysin (Syn) (Figures 3F and 3G), suggesting they were indeed sites of neurotransmitter release (and not just sites of VGluT2 accumulation). Taken together, these results demonstrate not only that collagen XVIII/endostatin is necessary for CF terminal formation in vivo, but also that endostatin is sufficient to induce presynaptic differentiation of these terminals in vitro.

To test whether the ability of endostatin to induce presynaptic differentiation was specific to CF axons, we repeated these experiments with dissociated granule cells. We failed to detect differences in the number of VGluT1-immunoreactive varicosities in the presence of recombinant endostatin (data not shown), suggesting that the ability of endostatin to induce presynaptic differentiation is cell type specific.

Cell PRESS
Open ACCESS

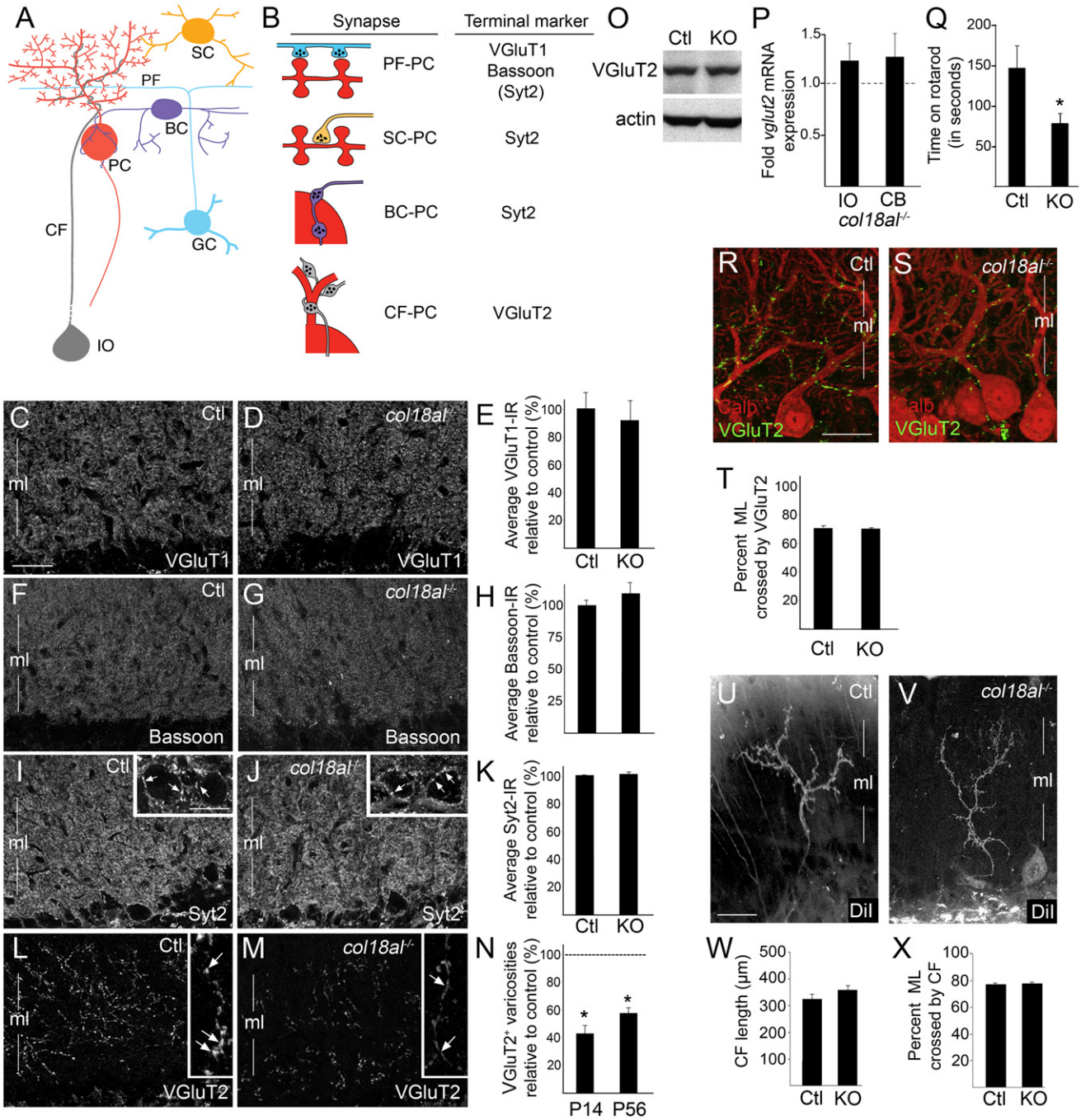

Figure 2. Collagen XVIII/Endostatin Is Necessary for the Organization of CF Terminals

(A) Neurons that synapse onto Purkinje cells (PC). GC, granule cell; IO, inferior olivary neuron; PF, parallel fiber; BC, basket cell; SC, stellate cell; CF, climbing fiber.

(B) Nerve terminal markers used to label terminals on PCs. Parentheses indicate Syt2 is present in a small set of PF terminals.

(C–M) Immunostaining for VGluT1 (C and D), Bassoon (F and G), Syt2 (I and J), and VGluT2 (L and M) in P56 control (Ctl) and *col18a1*$^{-/-}$ mutant cerebellum. Insets in (I and J) show high magnification of Syt2-positive axosomatic terminals on PCs (see arrows). Insets in (L and M) show high magnification of VGluT2 distribution in CFs: note its diffuse axonal distribution in *col18a1*$^{-/-}$ mutants; see arrows in (L and M). In (E), (H), and (K), average fluorescent intensity of VGluT1-, Bassoon-, and Syt2-immunoreactivity, respectively, in P56 control (Ctl) and mutants (KO). Data shown are means ± SEM; n > 4 mice per genotype. Scale bar in (C), 30 µm; in insets, 18 µm.

(N) Quantification of the total number of VGluT2-positive varicosities per image field in P14 and P56 *col18a1*$^{-/-}$ mutants compared to controls (dashed line). Data shown are mean ± SD; n > 4 mice per genotype. *Differ from litter mate controls at $p < 0.001$ by Student's t test.

(O) WBs show no difference in VGluT2 levels in P56 Ctl and KO cerebellum (CB). Actin was a loading control.

(P) qPCR of *vglut2* mRNA expression levels in P56 IO and CB of KOs and controls (dashed line). Data are mean ± SEM; n = 3.

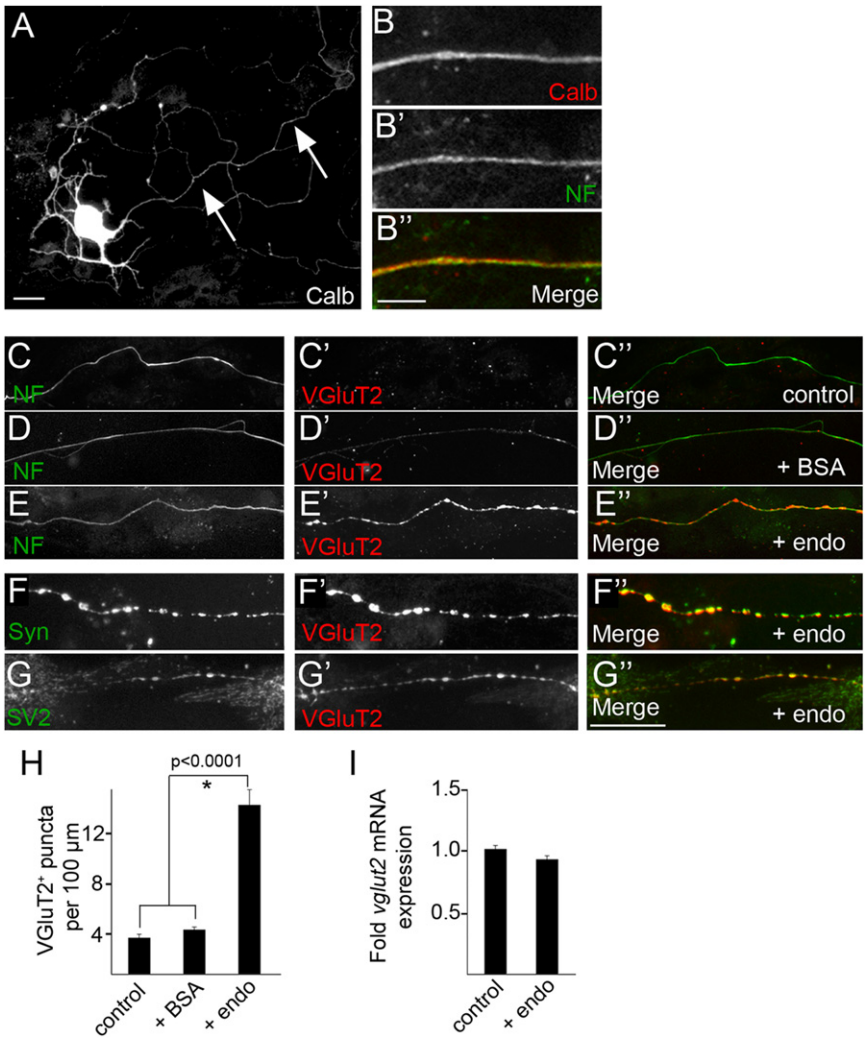

Figure 3. Endostatin Induces CF Terminal Formation In Vitro

(A) Inferior olivary neuron labeled by Calb-IHC in vitro. Arrows indicate CF axon. Scale bar, 25 μm.

(B and B′) CF axons were labeled in vitro with Calb- (B) and NF-IHC (B′). Scale bar in (B), 8 μm.

(C–E″) Control or BSA-treated CF axons had few VGluT2-immunoreactive synaptic varicosities; however, treatment with 0.1 μg/ml endostatin (endo) induced varicosity formation. Neurons were double labeled for NF (C–E) and VGluT2 (C′–E′). (C″–E″) represent the overlays of NF (green) and VGluT2 (red) labeling.

(F–G″) Endostatin-induced VGluT2-positive varicosities also contained other nerve-terminal-associated-proteins, such as synaptophysin (Syn in F) and SV2 (G). (F′ and G′) represent VGluT2 labeling and (F″ and G″) represent the merged overlays of VGluT2 (red) and either Syn or SV2 (green). Scale bar in (G″), 25 μm for (C–G″).

(H) Quantification of the number of VGluT2-positive synaptic varicosities in control and treated cultures. Data shown are means ± SD: n > 4 experiments in quadruplicate. *Differs from untreated or BSA-treated cultures at $p < 0.0001$ by Tukey-Kramer test for differences between means.

(I) qPCR revealed that application of endo did not significantly alter *vglut2* mRNA expression. Expression levels normalized to *gapdh*. Data shown are means ± SD; n > 3.

Endostatin Signals through α3β1 Integrins to Induce Synaptic Differentiation

We next explored what receptors might transduce these endostatin-induced signals in inferior olivary neurons. Outside of the nervous system, endostatin signals through αvβ3, αvβ5, and α5β1 integrin heterodimers (Ricard-Blum and Ballut, 2011)—all of which are expressed in the inferior olive (IO) (Figure S5E). More important, immunostaining for the β1 and β3 integrin subunits revealed that both were present on CF axons in vitro (Figures 4A and 4B; 99% ± 1% of NF-immunoreactive [NF-IR] axons contained β1 integrin, N = 3 experiments, n = 257 axons; 93% ± 3% of NF-IR axons contained β3 integrin, N = 3, n = 348). As the functions of β1- and β3-containing integrins are RGD-binding dependent, we tested whether endostatin-induced synaptogenesis could be blocked by RGD-containing peptides. Indeed, application of these peptides inhibited the ability of endostatin to induce CF terminal formation (Figures 4F–4H and 4K).

To determine which specific integrin heterodimer transduced endostatin-mediated signals, we explored the expression of the αv and α5 integrin subunits on CF axons. Neither was present on many CF axons (Figures 4C and 4D; 1% ± 1% of NF-IR axons contained αv integrin, N = 3, n = 335; 6% ± 1% of NF-IR axons contained α5 integrin, N = 3, n = 271). We therefore explored other integrin α subunits that form heterodimers with β1 or β3 subunits. One interesting candidate was the α3 integrin subunit: α3β1 integrin (the only integrin containing the α3 subunit) binds in an RGD-dependent fashion (Akula et al., 2002), is present on nerve terminals (Cohen et al., 2000), and links synaptic cleft molecules to active zone components within the nerve terminal (Carlson et al., 2010). Here we show that nearly all CF axons

(Q) Adult KOs exhibit impaired mobility on a rotating rod. Data are mean ± SEM; n = 10 Ctls and 13 KOs. *Differ from Ctls at $p < 0.05$ by Tukey HSD Test for differences between means.

(R and S) Immunostaining for Calb and VGluT2 in P21 Ctl and KO cerebella. Scale bar, 25 μm.

(T) Quantification of the percent of ML crossed by VGluT2-containing nerve terminals. Data are mean ± SEM; n = 60 measures from 3 mice.

(U and V) DiI-labeled CFs in the ML of P20 control and *col18a1*$^{-/-}$ mutant cerebellum. Scale bar, 30 μm.

(W and X) CF length in ML of KO and Ctl cerebella. In (X), quantification of the extent of ML crossed by the CFs in KO and Ctl cerebella. Data are means ± SEM; n = 26 control CFs and 23 mutants CFs.

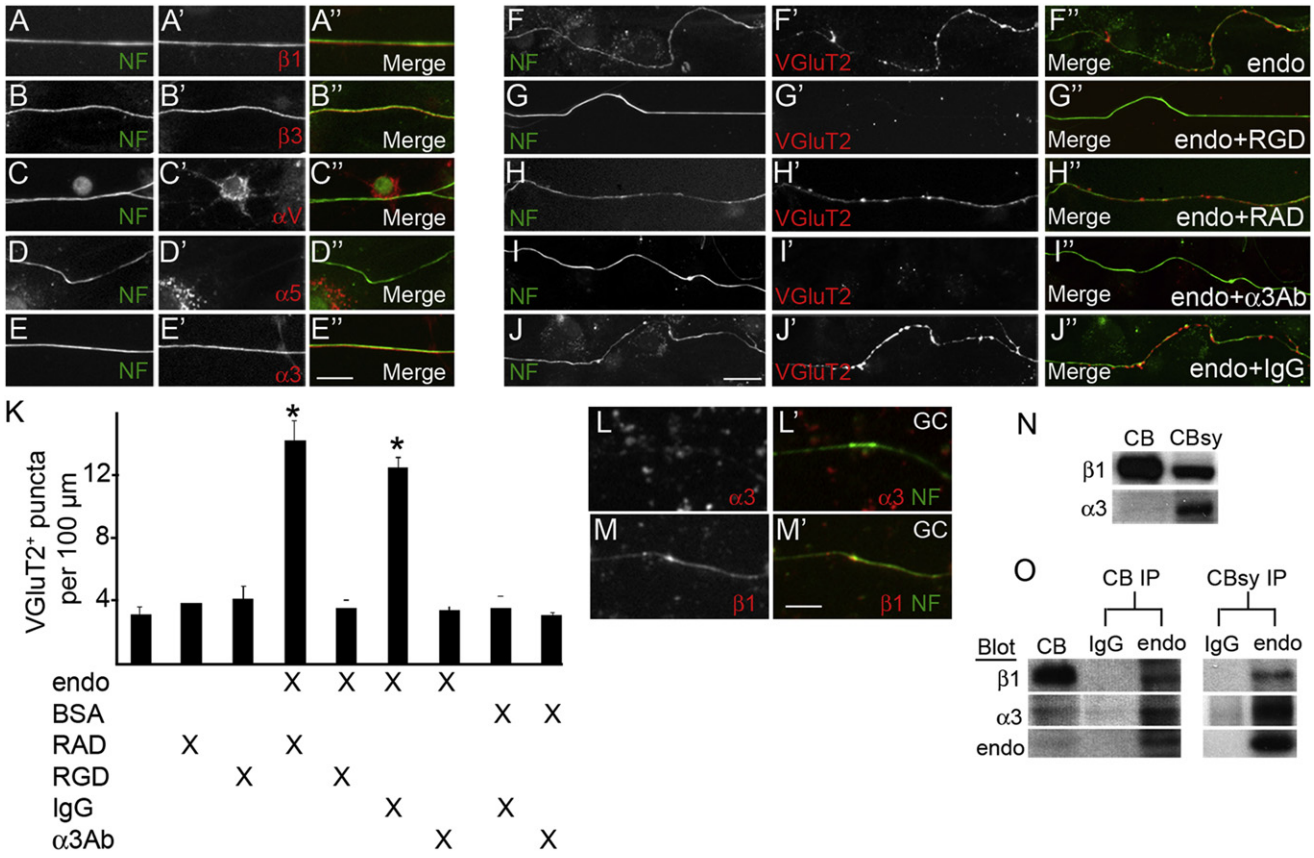

Figure 4. Endostatin Signals through α3β1 Integrins to Induce Nerve Terminal Formation In Vitro

(A–E″) IHC revealed that the β1, β3, and α3 integrin subunits were present on NF-positive CF axons in vitro. (A–E) depict NF immunolabeling; (A′–E′) depict integrin subunit labeling; (A″–E″) depicts the merged overlay of NF (green) and integrin (red) labeling. Scale bar, in (E), 20 μm.

(F–J″) Endostatin's ability to induce the formation of VGluT2-positive synaptic varicosities was inhibited by the application of 10 mM RGD peptides (G) or 25 μg/ml function blocking anti-α3 integrin antibodies (I), but not by control peptides (RAD in H) or antibodies (IgG in J). (F–J) depict NF immunolabeling; (F′–J′) depict VGluT2 labeling; (F″–J″) depicts the merged overlay of NF (green) and VGluT2 (red) labeling. Scale bar in (J), 25 μm.

(K) Quantification of the number of VGluT2-positive synaptic varicosities in cultures treated with combinations of endo, BSA, RAD peptides, RGD peptides, control IgG antibodies, and function blocking anti-α3 integrin antibodies. Data shown are means ± SD: n>4 experiments in quadruplicate. *Cultures treated with endo and either control peptides or antibodies differ from all other treatment groups at $p < 0.0001$ by Tukey-Kramer test for differences between means.

(L–M′) IHC revealed β1, but not α3, integrin subunits were present on cultured granule cell (GC) axons. (L and M) depict integrin immunolabeling; (L′ and M′) depict the merged overlay of NF (green) and integrin (red) labeling. Scale bar in (M), 15 μm.

(N) WBs demonstrate the presence of the α3 and β1 integrin subunits in cerebellar extracts (CB) and cerebellar synaptosome fractions (CBsy).

(O) Antibodies directed against endostatin immunoprecipitated the α3 and β1 integrin subunits from both CB and CBsy.

contained α3 integrin (Figure 4E; 99% ± 1% of NF-IR axons contained α3 integrin, N = 3, n = 335). The distribution of this integrin appeared evenly distributed throughout CF axons in control and endostatin-treated cultures (Figure 4E; data not shown). In addition to in vitro experiments, WBs revealed that α3β1 integrins were enriched in cerebellar synaptosome fractions (Figures 4N and S1D). To test whether endostatin signaled through α3β1 integrins in our assays, inferior olivary neurons were treated with function-blocking α3 integrin antibodies in conjunction with recombinant endostatin. Endostatin's ability to induce nerve terminal formation was abolished in the presence of these antibodies (Figures 4I–4K). In contrast to CF axons, few axons from dissociated granule cells contained α3 integrins (although they did contain β1 integrins) (Figures 4L and 4M; 5.2% ± 1% of NF-IR granule cell axons contained α3 integrin, N = 6, n = 256; 97.5% ± 0.9% of NF-IR axons contained β1 integrin, N = 6, n = 184). We suspect that differences in the expression of α3β1 integrins account for the cell-type-specific function of endostatin.

Finally, since α3β1–endostatin interactions had not been reported previously, we confirmed their interaction by immunoprecipitating these integrin subunits from cerebellar and synaptosome extracts with endostatin antibodies (Figure 4O). Surface plasmon resonance (SPR) binding assays were used to further demonstrate that α3β1 integrin directly binds endostatin with high affinity (K_D = 9.0 ± 3.6 nM, n = 2). The interaction data were best fit by a two-state interaction model (data not shown), similar to the binding of endostatin to α5β1 and αvβ3 integrins that we previously reported (Faye et al., 2009). Thus, α3β1 integrin is a receptor for endostatin.

The mammalian cerebellum has become a well-studied model for identifying synapse-specific signals that regulate neural circuit formation (Umemori et al., 2004; Scheiffele et al., 2000; Matsuda et al., 2010; Ango et al., 2004; Kalinovsky et al., 2011). In this study, we have added to our understanding of cerebellar circuit formation by identifying a matricryptin-releasing collagen that is necessary for the organization of CF terminals. While previous roles for collagen XVIII/endostatin have been described at the NMJ in worms, fish, and flies, we found that, despite its importance in cerebellum, collagen XVIII is dispensable for NMJ formation in mice (Figure S6). In addition to reporting a matricryptin that regulates neural circuit formation in the mammalian brain, our studies also provide a cellular mechanism that may help explain why collagen XVIII deficiency in Knobloch syndrome may predispose patients to neurological deficits (Suzuki et al., 2002).

EXPERIMENTAL PROCEDURES

Animals

Wild-type mice were obtained from Charles River Laboratories (Wilmington, MA, USA). Collagen XVIII null mice (*col18a1*$^{-/-}$) were described previously (Fukai et al., 2002). Standard rotarod experiments were performed on a Rotamex-5 (Columbus Instruments, Columbus, OH, USA) (Shiotsuki et al., 2010) with a 3 cm rod. At the onset of experiments, rods rotated at 1 rpm; however, every 15 s, the speed increased 1 rpm. The Rotamex-5 recorded the time at which each mouse fell. A total of 13 mutants and 10 littermate controls were analyzed. All analyses conformed to National Institutes of Health (NIH) guidelines and were carried out under protocols approved by the Virginia Commonwealth University (VCU) Institutional Animal Care and Use Committee.

RT-PCR

RNA isolation, RT-PCR, and real-time quantitative PCR were all performed as previously described (Su et al., 2010). Primer sequences can be found in the Extended Experimental Procedures.

Immunohistochemistry

Fluorescent immunohistochemistry (IHC) was performed on 16 μm cryosectioned paraformaldehyde (PFA)-fixed brain tissue or cultured neurons as described previously (Fox et al., 2007; Su et al., 2010). Images were acquired on a Zeiss AxioImager A1 fluorescent microscope or a Leica SP2 confocal microscope. When comparing different ages of tissues or between genotypes, we acquired images with identical parameters. Tissues from at least four animals were analyzed for each genotype, and IHC analysis was performed on at least eight random fields (875 μm × 650 μm) per animal. Total number of puncta per field was counted manually. Average fluorescent intensities were measured in ImageJ as previously described (Su et al., 2010). A list of the antibodies and additional details can be found in the Extended Experimental Procedures.

In Situ Hybridization

Riboprobe generation and in situ hybridization (ISH) were performed as described previously (Su et al., 2010). Sense and antisense riboprobes against *col18a1* were generated from a 967-base-pair fragment of *col18a1*, corresponding to nucleotides (nt) 3190–4156, and were hydrolyzed to 500 nt.

WB and Immunoprecipitation Analysis

WBs and immunoprecipitation analyses (IPs) were performed as described previously (Fox and Sanes, 2007; Su et al., 2010). A previously described rabbit polyclonal antibody against endostatin was used for IPs (Faye et al., 2010). Additional information can be found in the Extended Experimental Procedures.

In Vitro Cultures

IOs were dissected from P0 mouse brains and were digested in 0.25% trypsin. Trypsin was inactivated, and tissue was transferred to Neurobasal medium containing 0.5 mM L-glutamine, 25 μM L-glutamate, 10 μg/ml gentamicin, and 10% fetal bovine serum (FBS). Single-cell suspensions were plated on poly-L-lysine-treated chamber slides and were cultured for 4 days. After 2 additional days in Neurobasal medium containing 0.5 mM L-glutamine, 10 μg/ml gentamicin, and B27 supplement, IO cells were treated with endostatin (0.1 μg/ml; ProSpec Inc.), bovine serum albumin (BSA) (0.1 μg/ml), RGD (10 μM), RAD (10 μM), integrin α3 antibody (25 μg/ml; Millipore), and/or mouse immunoglobulin G (IgG) (25 μg/ml). After 2 days, cells were fixed with 4% PFA and immunostained. Granule cell cultures were generated as previously described (Umemori et al., 2004) and were treated as described earlier.

CF Labeling

CF labeling was performed using the method of Kiyohara et al. (2003). Brains were fixed in 4% PFA and DiI (0.5%–1.0% in dimethyl sulfoxide; DMSO) was injected into the inferior cerebellar peduncle. Brains were incubated in 4% PFA at 37°C for 3 weeks, sectioned with a vibratome, and imaged with a Leica SP2 scanning confocal microscope. CF arbors and the extent of the molecular layer were measured in ImageJ.

SPR Binding Assays

The SPR binding assays were performed in a Biacore T200 instrument (GE Healthcare). Recombinant human endostatin was covalently immobilized to the dextran matrix of a CM5 sensor chip via its primary amine groups as described previously (Faye et al., 2009). Sensorgrams collected on the control flow cell were automatically subtracted from the sensorgrams obtained on immobilized endostatin to yield specific binding responses. Kinetic and affinity constants were calculated by injecting several concentrations of α3β1 integrin (Millipore). Complexes were dissociated with 2 M NaCl. Rate constants were calculated using Biacore T200 software.

SUPPLEMENTAL INFORMATION

Supplemental Information includes Extended Experimental Procedures and six figures and can be found with this article online at http://dx.doi.org/10.1016/j.celrep.2012.07.001.

LICENSING INFORMATION

ACKNOWLEDGMENTS

We thank Drs. J.R. Sanes, J.F. Strauss III, H. Umemori, and G. Valdez for comments on the manuscript; Dr. Bjorn Olsen (Harvard) for *col18a1*$^{-/-}$ mice; R. Salza (University Lyon, Lyon, France) for help with binding assays; and Christophe Quétard (GE Healthcare, Lyon, France) for providing access to a Biacore T200 system. This work was supported by an A.D. Williams Grant (M.A.F.) and National Institutes of Health (NIH) Grant EY021222 (M.A.F.). Microscopy was performed at the VCU Microscopy Facility supported by an NIH Core Grant (NS047463).

Received: December 1, 2011
Revised: April 5, 2012
Accepted: July 2, 2012
Published online: August 9, 2012

REFERENCES

Ackley, B.D., Kang, S.H., Crew, J.R., Suh, C., Jin, Y., and Kramer, J.M. (2003). The basement membrane components nidogen and type XVIII collagen regulate organization of neuromuscular junctions in Caenorhabditis elegans. J. Neurosci. *23*, 3577–3587.

Akula, S.M., Pramod, N.P., Wang, F.Z., and Chandran, B. (2002). Integrin alpha3beta1 (CD 49c/29) is a cellular receptor for Kaposi's

sarcoma-associated herpesvirus (KSHV/HHV-8) entry into the target cells. Cell *108*, 407–419.

Ango, F., di Cristo, G., Higashiyama, H., Bennett, V., Wu, P., and Huang, Z.J. (2004). Ankyrin-based subcellular gradient of neurofascin, an immunoglobulin family protein, directs GABAergic innervation at purkinje axon initial segment. Cell *119*, 257–272.

Carlson, S.S., Valdez, G., and Sanes, J.R. (2010). Presynaptic calcium channels and α3-integrins are complexed with synaptic cleft laminins, cytoskeletal elements and active zone components. J. Neurochem. *115*, 654–666.

Cohen, M.W., Hoffstrom, B.G., and DeSimone, D.W. (2000). Active zones on motor nerve terminals contain alpha 3beta 1 integrin. J. Neurosci. *20*, 4912–4921.

Egles, C., Claudepierre, T., Manglapus, M.K., Champliaud, M.F., Brunken, W.J., and Hunter, D.D. (2007). Laminins containing the beta2 chain modulate the precise organization of CNS synapses. Mol. Cell. Neurosci. *34*, 288–298.

Faye, C., Moreau, C., Chautard, E., Jetne, R., Fukai, N., Ruggiero, F., Humphries, M.J., Olsen, B.R., and Ricard-Blum, S. (2009). Molecular interplay between endostatin, integrins, and heparan sulfate. J. Biol. Chem. *284*, 22029–22040.

Faye, C., Inforzato, A., Bignon, M., Hartmann, D.J., Muller, L., Ballut, L., Olsen, B.R., Day, A.J., and Ricard-Blum, S. (2010). Transglutaminase-2: a new endostatin partner in the extracellular matrix of endothelial cells. Biochem. J. *427*, 467–475.

Fox, M.A., and Umemori, H. (2006). Seeking long-term relationship: axon and target communicate to organize synaptic differentiation. J. Neurochem. *97*, 1215–1231.

Fox, M.A., and Sanes, J.R. (2007). Synaptotagmin I and II are present in distinct subsets of central synapses. J. Comp. Neurol. *503*, 280–296.

Fox, M.A., Sanes, J.R., Borza, D.B., Eswarakumar, V.P., Fässler, R., Hudson, B.G., John, S.W., Ninomiya, Y., Pedchenko, V., Pfaff, S.L., et al. (2007). Distinct target-derived signals organize formation, maturation, and maintenance of motor nerve terminals. Cell *129*, 179–193.

Fremeau, R.T., Jr., Troyer, M.D., Pahner, I., Nygaard, G.O., Tran, C.H., Reimer, R.J., Bellocchio, E.E., Fortin, D., Storm-Mathisen, J., and Edwards, R.H. (2001). The expression of vesicular glutamate transporters defines two classes of excitatory synapse. Neuron *31*, 247–260.

Fukai, N., Eklund, L., Marneros, A.G., Oh, S.P., Keene, D.R., Tamarkin, L., Niemelä, M., Ilves, M., Li, E., Pihlajaniemi, T., and Olsen, B.R. (2002). Lack of collagen XVIII/endostatin results in eye abnormalities. EMBO J. *21*, 1535–1544.

Kalinovsky, A., Boukhtouche, F., Blazeski, R., Bornmann, C., Suzuki, N., Mason, C.A., and Scheiffele, P. (2011). Development of axon-target specificity of ponto-cerebellar afferents. PLoS Biol. *9*, e1001013.

Kiyohara, Y., Endo, K., Ide, C., and Mizoguchi, A. (2003). A novel morphological technique to investigate a single climbing fibre synaptogenesis with a Purkinje cell in the developing mouse cerebellum: DiI injection into the inferior cerebellar peduncle. J. Electron Microsc. (Tokyo) *52*, 327–335.

Ksiazek, I., Burkhardt, C., Lin, S., Seddik, R., Maj, M., Bezakova, G., Jucker, M., Arber, S., Caroni, P., Sanes, J.R., et al. (2007). Synapse loss in cortex of agrin-deficient mice after genetic rescue of perinatal death. J. Neurosci. *27*, 7183–7195.

Mason, C.A., and Gregory, E. (1984). Postnatal maturation of cerebellar mossy and climbing fibers: transient expression of dual features on single axons. J. Neurosci. *4*, 1715–1735.

Matsuda, K., Miura, E., Miyazaki, T., Kakegawa, W., Emi, K., Narumi, S., Fukazawa, Y., Ito-Ishida, A., Kondo, T., Shigemoto, R., et al. (2010). Cbln1 is a ligand for an orphan glutamate receptor delta2, a bidirectional synapse organizer. Science *328*, 363–368.

Meyer, F., and Moussian, B. (2009). Drosophila multiplexin (Dmp) modulates motor axon pathfinding accuracy. Dev. Growth Differ. *51*, 483–498.

Muragaki, Y., Timmons, S., Griffith, C.M., Oh, S.P., Fadel, B., Quertermous, T., and Olsen, B.R. (1995). Mouse Col18a1 is expressed in a tissue-specific manner as three alternative variants and is localized in basement membrane zones. Proc. Natl. Acad. Sci. USA *92*, 8763–8767.

Ricard-Blum, S., and Ballut, L. (2011). Matricryptins derived from collagens and proteoglycans. Front. Biosci. *16*, 674–697.

Richter, K., Langnaese, K., Kreutz, M.R., Olias, G., Zhai, R., Scheich, H., Garner, C.C., and Gundelfinger, E.D. (1999). Presynaptic cytomatrix protein bassoon is localized at both excitatory and inhibitory synapses of rat brain. J. Comp. Neurol. *408*, 437–448.

Scheiffele, P., Fan, J., Choih, J., Fetter, R., and Serafini, T. (2000). Neuroligin expressed in nonneuronal cells triggers presynaptic development in contacting axons. Cell *101*, 657–669.

Schneider, V.A., and Granato, M. (2006). The myotomal diwanka (lh3) glycosyltransferase and type XVIII collagen are critical for motor growth cone migration. Neuron *50*, 683–695.

Shiotsuki, H., Yoshimi, K., Shimo, Y., Funayama, M., Takamatsu, Y., Ikeda, K., Takahashi, R., Kitazawa, S., and Hattori, N. (2010). A rotarod test for evaluation of motor skill learning. J. Neurosci. Methods *189*, 180–185.

Sotelo, C. (2008). Viewing the cerebellum through the eyes of Ramón Y Cajal. Cerebellum *7*, 517–522.

Su, J., Gorse, K., Ramirez, F., and Fox, M.A. (2010). Collagen XIX is expressed by interneurons and contributes to the formation of hippocampal synapses. J. Comp. Neurol. *518*, 229–253.

Suzuki, O.T., Sertié, A.L., Der Kaloustian, V.M., Kok, F., Carpenter, M., Murray, J., Czeizel, A.E., Kliemann, S.E., Rosemberg, S., Monteiro, M., et al. (2002). Molecular analysis of collagen XVIII reveals novel mutations, presence of a third isoform, and possible genetic heterogeneity in Knobloch syndrome. Am. J. Hum. Genet. *71*, 1320–1329.

Terauchi, A., Johnson-Venkatesh, E.M., Toth, A.B., Javed, D., Sutton, M.A., and Umemori, H. (2010). Distinct FGFs promote differentiation of excitatory and inhibitory synapses. Nature *465*, 783–787.

Umemori, H., Linhoff, M.W., Ornitz, D.M., and Sanes, J.R. (2004). FGF22 and its close relatives are presynaptic organizing molecules in the mammalian brain. Cell *118*, 257–270.